International Journal of Nanomedicine

Dovepress
open access to scientific and medical research

Open Access Full Text Article

ORIGINAL RESEARCH

Real-time analysis of dual-display phage immobilization and autoantibody screening using quartz crystal microbalance with dissipation monitoring

This article was published in the following Dove Press journal:
International Journal of Nanomedicine
19 August 2015
Number of times this article has been viewed

Kaushik Rajaram[1]
Patricia Losada-Pérez[2,3]
Veronique Vermeeren[1]
Baharak Hosseinkhani[1]
Patrick Wagner[2,4]
Veerle Somers[1]
Luc Michiels[1]

[1]Biomedical Research Institute (BIOMED), Hasselt University, Hasselt, [2]Institute for Materials Research (IMO), Hasselt University, [3]IMEC vzw, Division IMOMEC, Diepenbeek, [4]Soft Matter and Biophysics Section, Department of Physics and Astronomy, KU Leuven, Leuven, Belgium

Abstract: Over the last three decades, phage display technology has been used for the display of target-specific biomarkers, peptides, antibodies, etc. Phage display-based assays are mostly limited to the phage ELISA, which is notorious for its high background signal and laborious methodology. These problems have been recently overcome by designing a dual-display phage with two different end functionalities, namely, streptavidin (STV)-binding protein at one end and a rheumatoid arthritis-specific autoantigenic target at the other end. Using this dual-display phage, a much higher sensitivity in screening specificities of autoantibodies in complex serum sample has been detected compared to single-display phage system on phage ELISA. Herein, we aimed to develop a novel, rapid, and sensitive dual-display phage to detect autoantibodies presence in serum samples using quartz crystal microbalance with dissipation monitoring as a sensing platform. The vertical functionalization of the phage over the STV-modified surfaces resulted in clear frequency and dissipation shifts revealing a well-defined viscoelastic signature. Screening for autoantibodies using antihuman IgG-modified surfaces and the dual-display phage with STV magnetic bead complexes allowed to isolate the target entities from complex mixtures and to achieve a large response as compared to negative control samples. This novel dual-display strategy can be a potential alternative to the time consuming phage ELISA protocols for the qualitative analysis of serum autoantibodies and can be taken as a departure point to ultimately achieve a point of care diagnostic system.

Keywords: dual-display phage, surface plasmon resonance, quartz crystal microbalance, dissipation monitoring, streptavidin-binding protein, rheumatoid arthritis

Introduction

In diagnostic sectors an immense demand has been raised to discover disease-related biomarkers. The most commonly used bioreceptors are antibodies, nucleic acids, proteins, whole cells, or microorganisms. Recently, bacteriophages have emerged as versatile bioreceptors in the development of diagnostic biosensors due to their high thermal and chemical stability and robustness.[1–3] The phage can be directly used as a probe when they are modified to display disease-related antigens on its surface.[4] The phage production is also cost-effective, and they can be produced in sufficient numbers by just infecting a bacterial host. The phage could be used to display different types of peptides, proteins, and antibodies to be employed in affinity selection of target-specific phage particles.[1,2,5–8]

Current advances in biosensors are providing the possibility for immobilizing bioreceptor molecules in a site-directed pattern while retaining their intact

Correspondence: Kaushik Rajaram
Biomedical Research Institute (BIOMED), Hasselt University, Martelarenlaan 42, 3500 Hasselt, Belgium
Email rkaushikmbt@gmail.com

Patricia Losada-Pérez
Institute for Materials Research (IMO), Hasselt University, Wetenschapspark 1, B-3590 Diepenbeek, Belgium
Email patricia.losadaperez@uhasselt.be

structure and native biological function.[9] As recently reported, the oriented immobilization of bacteriophages on a sensing platform resulted in a higher sensitivity in the detection of autoantibodies in serum samples.[6] A main drawback of bacteriophages-based diagnostic assays is the nonspecific adsorption of proteins, leading to a high background signal and decreasing sensitivity. Due to the lack of a specific strategy to bring the phage onto a sensing platform, most of the phage-based assays are limited to an ELISA format.[10] However, if complex substances, such as serum, are used to screen for targets, phage ELISA lacks sensitivity due to nonspecific binding of interfering serum components.[11]

To overcome this problem, we designed a dual-display phage system including an autoantigenic target UH-RA.21 as a biomarker and streptavidin (STV)-binding protein (SBP) as capturing peptide, both being displayed at opposite ends of a filamentous phage.[12] This approach resulted in a higher sensitivity of signal detection assays using STV-coated magnetic beads. Specifically, the dual phage displayed a biomarker (autoantigenic target UH-RA.21 specific for rheumatoid arthritis) fused to a coat protein pVI at one end and an anchoring SBP fused to a coat protein pVII at the other end. This system allowed us to isolate the autoantibodies from the complex serum sample by using STV-coated magnetic beads followed by magnetic capturing of the phage, thus increasing the sensitivity in phage ELISA assay. In this context, introducing the dual-display phage as a bioreceptor in a sensing platform can present a promising technique for rapid, label-free screening and highly specific diagnosis of rheumatoid arthritis and extend its use to other diseases. In this regard, real-time monitoring of the dual-display phage immobilization onto an adequate biosensing platform is necessary for evaluating its binding ability and stability. Among the different existing sensing platforms, quartz crystal microbalance with dissipation monitoring (QCM-D) fulfills the above-mentioned requirements and stands as a versatile, highly sensitive, label free and real-time technology.[13–15]

In this work, we present a twofold study of a dual-display phage displaying SBP using QCM-D. On the one hand, we evaluate the binding ability and stability of the dual-display system onto chemically modified sensors via STV–SBP binding from one end. On the other hand, we monitored the screening of autoantibodies in UH-RA.21 antibody-positive serum sample using the opposite end functionality, a rheumatoid arthritis biomarker. For assessing the binding ability and stability, we followed the interaction of the dual-display phage onto STV-modified sensors by QCM-D and by complementary surface plasmon resonance (SPR) measurements. In particular, we examined the binding of four phages with different end modifications to STV-modified Au-coated QCM-D sensors and to STV-modified SPR chips. For monitoring the screening of autoantibodies in UH-RA.21 antibody-positive serum sample, we immobilized antihuman IgG onto the QCM-D sensors and isolated the specific autoantibodies from the serum samples through STV-coated magnetic beads modified with the SBP and the biomarker displaying phage. This dual-display phage-based real time and label-free sensing methodology can open up a new avenue in the future diagnostics.

Materials and methods

Materials

Four different types of phage SR21 (displaying SBP and UH-RA.21), SB (displaying SBP), CR21 (displaying UH-RA.21), and CB (empty [negative control]) were prepared previously using the combination of helper plasmid (with or without SBP) and phagemid (with or without UH-RA.21).[12] STV (SO677) was obtained from Sigma Aldrich (Diegem, Belgium). STV-coated magnetic beads were purchased from Thermo Fisher Scientific (Waltham, MA, USA). Serum autoantibodies (UH-RA.21 antibody positive) and negative control (UH-RA.21 antibody negative) serum were produced in house. Au-coated AT-cut quartz crystals (diameter 14 mm, thickness 0.3 mm, surface roughness 3 nm, and resonant frequency 4.95 MHz QCM-D crystals) were purchased from Q-Sense, Sweden.

Phage complex preparation using phage, serum, and streptavidin-coated magnetic beads

SR21 phage diluted to 10^{11} CFU/mL in 1× phosphate-buffered saline (PBS) buffer were preincubated with 100× diluted serum samples in 1× PBS buffer with gentle shaking at 100 rpm for 1 hour at 37°C. Then, 1 µL of 10 µg/µL ($3–6\times10^6$) STV-coated magnetic beads (Thermo Fisher Scientific) was added to the phage serum mixture and incubated for 30 minutes at 37°C while shaking. The phage serum bead complexes were captured with a magnetic field and washed twice with 1× PBS to remove unbound phage and remaining serum. Finally, captured phage were collected and resuspended in 1 mL of 1× PBS.

Quartz crystal microbalance with dissipation monitoring

The Au-coated quartz sensors were cleaned with a 5:1:1 mixture of Milli Q water (conductivity of 0.055 S cm^{-1} at 25°C), ammonia, and hydrogen peroxide and were ultraviolet ozone treated with a Digital PSD series ultraviolet ozone system from Novascan for 15 minutes, followed by rinsing in Milli Q water and drying with N_2. For the current measurements, we have used QCM-D on a Q-Sense E4 instrument (Gothenburg, Sweden) to monitor the frequency shift Δf and the dissipation change ΔD. The changes in Δf and in ΔD were monitored at three different overtones (from third to seventh) in a continuous flow mode with a rate of 100 µL/min over plain Au-coated QCM-D sensors. All measurements were carried out at 20°C.

Characterization of SBP display in phage

The procedure carried out for each type of phage can be summarized as follows. After a baseline in 1× PBS buffer was established, 25 µg/mL of STV in 1× PBS buffer was injected until saturation was observed. 1× PBS buffer was flushed to remove unbound STV from the surface and to check the stability of the adsorbed layer. Then, 1×10^{11} CFU/mL of phage samples were injected for 20 minutes and flushed with 1× PBS once more to remove the unbound phage from the crystals.

Screening of autoantibodies in the serum samples

First, antihuman IgG was immobilized on the sensing platform by introducing 10 µg/mL antihuman IgG in 1× PBS buffer over plain Au-coated QCM-D sensors with a flow rate of 100 µL/min. After saturation of the sensor surface, unbound antihuman IgG was removed by flushing the system with 1× PBS buffer. Afterward, the phage complexes were introduced with a flow rate of 100 µL/min in the corresponding cells and subsequently rinsed with 1× PBS after saturation was completed. As previously described, the positive complexes were prepared by preincubating phage, UH-RA.21 antibody-positive serum sample and the subsequent isolation of bound phage, and autoantibodies using STV-coated magnetic beads.

Surface plasmon resonance

All the four phage samples have been diluted to 1×10^{11} CFU/mL in 1× PBS buffer, and the predesigned immobilization protocols have been used while keeping 1× PBS as running buffer with a flow rate of 12 µL/min and the flow duration of 500 seconds. Flow cell 1 (FC 1) treated with CR21, FC 2 with SR21, FC 3 with CB, and the FC 4 with SB phage. The bound response values have been monitored for all four phages. SA chips of Biacore are three-dimensional chips containing a dextran matrix preimmobilized with STV. The dual-display phage's affinity binding toward STV was monitored on BIACORE STV functionalized chips SA sensor chips of Biacore (GE Healthcare, Uppsala, Sweden). SPR measurements were performed on a Biacore T200 instrument (GE Healthcare Bio-Sciences AB, Uppsala, Sweden) in PBS-running buffer at a constant temperature of 25°C.

Results and discussion

We divide this section into two parts corresponding to the two main goals of this work: 1) to monitor the real-time binding of the dual-display phage from the SBP modified end onto STV-functionalized sensors and to evaluate the viscoelastic properties of the layer, 2) to monitor the real-time performance of the dual-display phage in screening for autoantibodies in the UH-RA.21 antibody-positive serum versus UH-RA.21 antibody-negative serum samples in a QCM-D platform.

Binding characteristic of phage to the STV-functionalized sensor surfaces

QCM-D results

QCM-D is an acoustic surface sensitive technique based on the inverse piezoelectric effect, in which the application of an AC voltage over the sensor electrodes causes the piezoelectric quartz crystal to oscillate at its acoustic resonance frequency. The adsorption of a sample is reflected as a shift in the resonance frequency (Δf) and the energy dissipation factor (ΔD). The former is related to mass changes over the sensor surface[16] while the later accounts for the energy dissipation due to the presence of the adsorbed layer.[17]

Figure 1 displays the Δf and ΔD responses upon STV adsorption and subsequent binding of SBP displaying phage SR21 (positive) and non-SBP displaying phage CR21 (negative). Upon binding of STV, Δf decreases to ~–20 Hz, indicating the physical adsorption and formation of a STV layer onto the Au-coated sensor. The STV layer is quite rigid, judging from the values of ΔD ~0 and from the fact that the overtones in both Δf and ΔD overlap.[17,18] After PBS buffer flushing, the level of Δf and ΔD hardly changed indicating that the STV layer was quite stable. Subsequent introduction of the SBP displaying phage (SR21) into the system caused large shifts in both Δf and ΔD. The Δf response decreases

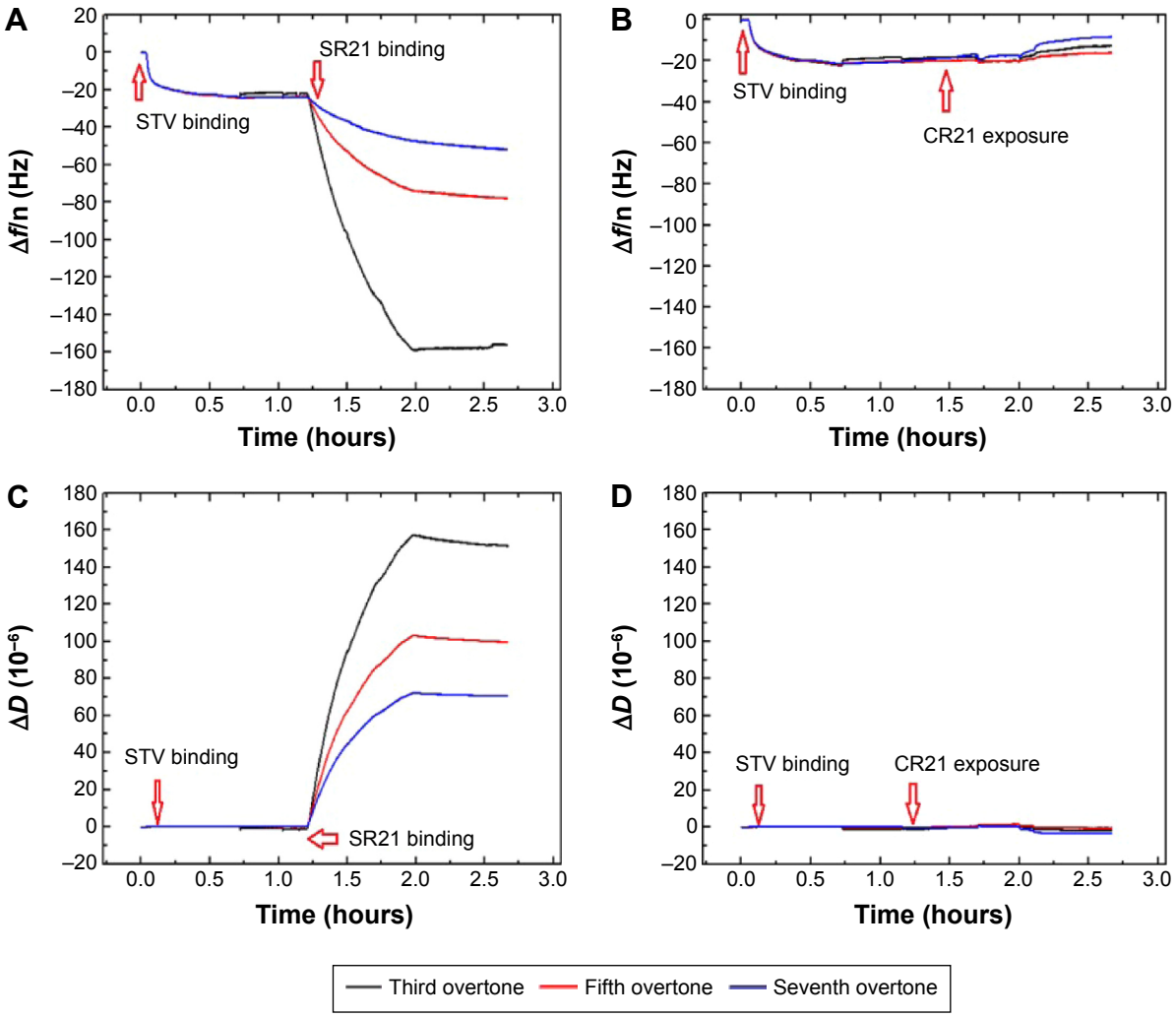

Figure 1 Δf and ΔD responses upon STV adsorption and subsequent binding of SBP displaying phage SR21 (**A** and **C**) and non-SBP displaying CR21 (**B** and **D**) to the Au-coated QCM-D sensors. The red arrows indicate the time of addition of the sample.
Abbreviations: STV, streptavidin; SBP, streptavidin-binding protein; QCM-D, quartz crystal microbalance with dissipation monitoring.

to ~−180 Hz, reflecting the binding event of SBP displaying phage SR21. In addition, the increase in ΔD indicated that the adsorbed SBP displayed phage layer is very dissipative. In turn, the introduction of the negative sample (non-SBP displaying phage CR21) hardly induced any change in the level of Δf and ΔD, if any, it slightly destabilized the STV layer, and removed adsorbed STV, as concluded from the slight increase (decrease) in Δf (ΔD) response (Figure 1B and D).

An additional $\Delta D - \Delta f$ plot shown in Figure 2 eliminates time as an explicit adsorption parameter and provides insights into the viscoelastic nature of the formed adlayers.[19] Specifically, the slope of the line between the initial and final point of adsorption, $k_{D-f} = \Delta D/\Delta f$ scales differently with different adlayer conformations. This means that rigid and compact layers yield low k_{D-f} values, whereas bulky and diffuse layers yield high k_{D-f} values.[19] Figure 2A shows the different slopes upon STV and SBP displaying phage adsorption. As it can be observed, adsorption of STV yields a k_{D-f}=−0.01, while adsorption of SBP displaying phage k_{D-f}=−2.09. As anticipated before, the STV layer is a rigid and compact layer, while the phage is a soft biomolecule in a likely vertical conformation. Though water is entrapped in both layers, the phage allows a larger amount of water molecules within the layer thus showing large energy dissipation. Furthermore, the effective thickness before and after phage addition was calculated using the Voigt based model consisting of an elastic element (spring) in parallel with a viscous element (dashpot).[18,20,21] The data of several overtones (third to seventh) were fitted using the software Qtools (Q-Sense AB, Sweden) keeping as fixed parameters the density and the viscosity of the fluid as 1.0 g·cm^{-3} and

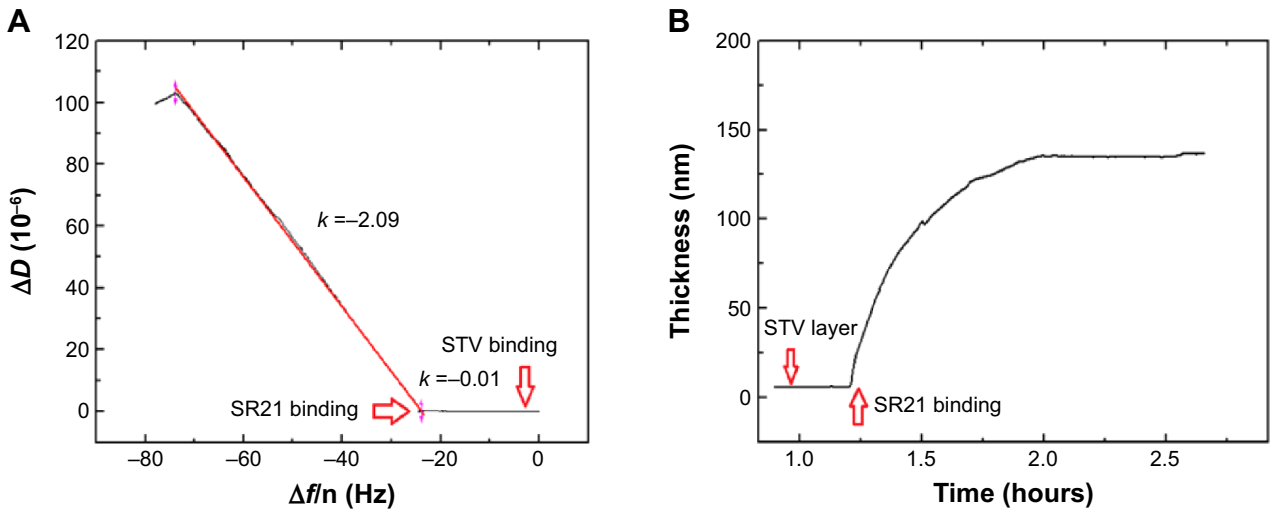

Figure 2 Kinetic study on the phage immobilization.
Notes: (**A**) $\Delta D - \Delta f$ plots showing adsorption of STV (black solid line) and SBP displaying phage SR21 (red solid line). (**B**) Estimated thickness of the SBP displaying phage SR21 layer. The red arrows indicate the time of addition of the sample.
Abbreviations: STV, streptavidin; SBP, streptavidin-binding protein.

1 mPa·s, respectively. The obtained values should be taken as an approximation, since we ignore the density of the STV and of the dual-display phage layers. However, the significant increase in thickness (Figure 2B) upon phage binding is due to the most likely vertical configuration of the phage. In order to assess the speed of adsorption of the two processes, the Δf responses of the separate events were fitted to a single exponential decay:

$$\Delta f = \Delta f_0 + Ae^{-t/\tau} \quad (1)$$

where A is the amplitude and τ is the time constant. As it can be observed in Figure 3, the adsorption of STV onto the Au-coated QCM-D sensors is fast (τ ~329 seconds), while the SBP displaying phage is more gradual and slower (τ ~1,750 seconds). Although not shown here, the remaining phages, positive single-display phage SB and negative phage CB, behaved in the same way as their positive and negative counter parts, SR21 phage and CR21 phage, respectively (Figures S1 and S2).

SPR results

The physical principle behind SPR is based on the change of the optical properties of the medium upon sample adsorption, which translates in a shift in the reflectivity versus angle dip.[22] STV can form affinity binding with biotin or with SBP, and one can expect it to happen very rapidly.[23,24] Since STV and SBP binding is mostly irreversible, the chips cannot be reused or regenerated. 1×10^{11} CFU/mL of phage samples were introduced over the corresponding FC's at a rate of 12 µL/min, and the binding response was immediately observed. Figure 4 shows a comparison of the binding response between positive and negative samples. As expected, positive samples display a much larger binding affinity with higher stability, whereas for both negative phage samples, response bound went to negative values and back to the baseline after buffer addition (see insert in Figure 4).

Screening of autoantibodies in serum using QCM-D

The presence of autoantibodies in serum was detected based on their biointerface characterization (Δf and ΔD)

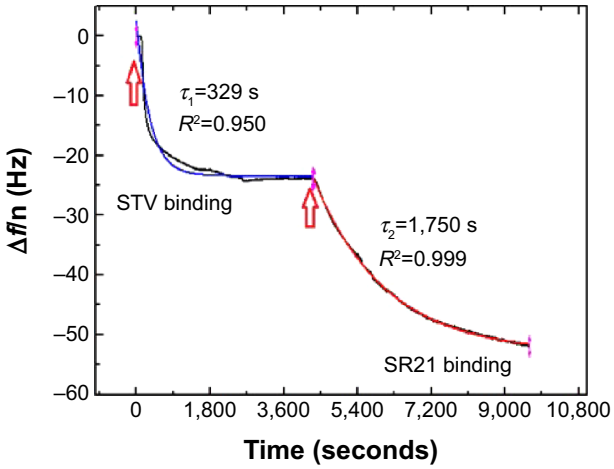

Figure 3 Kinetics of adsorption of STV to Au-coated QCM-D sensors and subsequent binding of SBP displaying phage SR21.
Notes: The blue and red solid lines represent the fits to Equation 1: $\Delta f = \Delta f_0 + Ae^{-t/\tau}$. The black line is experimental data. The red arrows indicate the time of addition of the sample.
Abbreviations: STV, streptavidin; QCM-D, quartz crystal microbalance with dissipation monitoring; SBP, streptavidin-binding protein; *A*, amplitude; τ, time constant.

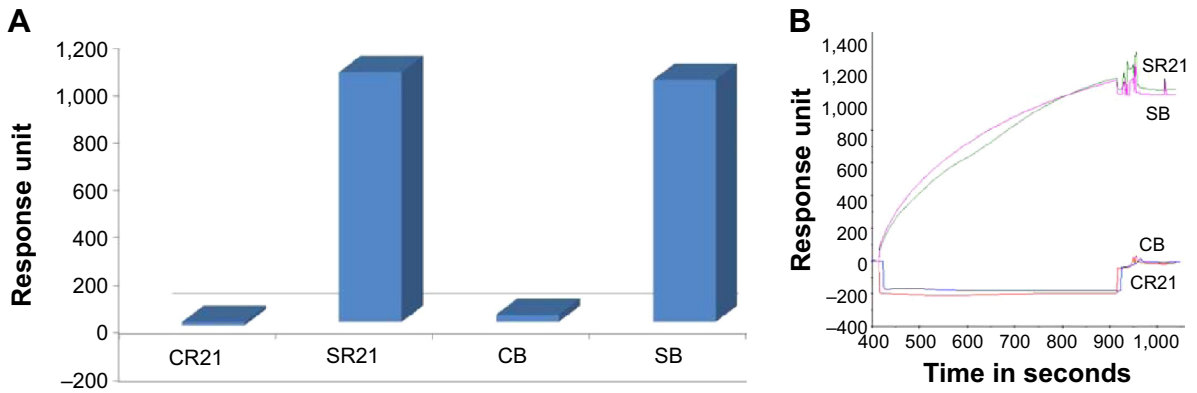

Figure 4 Characterization of SBP displaying phage binding to the streptavidin surfaces using SPR.
Notes: (**A**) The SBP displaying phage (SR21 and SB) binds to the STV surface of a SA chip and non-SBP displaying phage (CR21, CB) shows no binding pattern. (**B**) shows the real-time binding curves, and SBP displayers show high stability when flushing with buffer while the negatives revert back to the base line due to the buffer effect.
Abbreviations: SBP, streptavidin-binding protein; SPR, surface plasmon resonance; STV, streptavidin.

on QCM-D. Figure 5 shows the Δf and ΔD responses upon antihuman IgG adsorption and subsequent binding of dual display positive complex SR21 (left panels) and negative complex CR21 (right panels). In the first step, the adsorption value of antihuman IgG over Au-coated sensors yielded Δf ~−30 Hz and ΔD ~0.75×10^{-6}. The small ΔD value indicates that the layer of antihuman IgG is quite rigid, in addition to this, during the washing step with PBS buffer, Δf and ΔD values remained the same. The physical adsorption in Figure 5 shows that the binding of antihuman IgG (the first

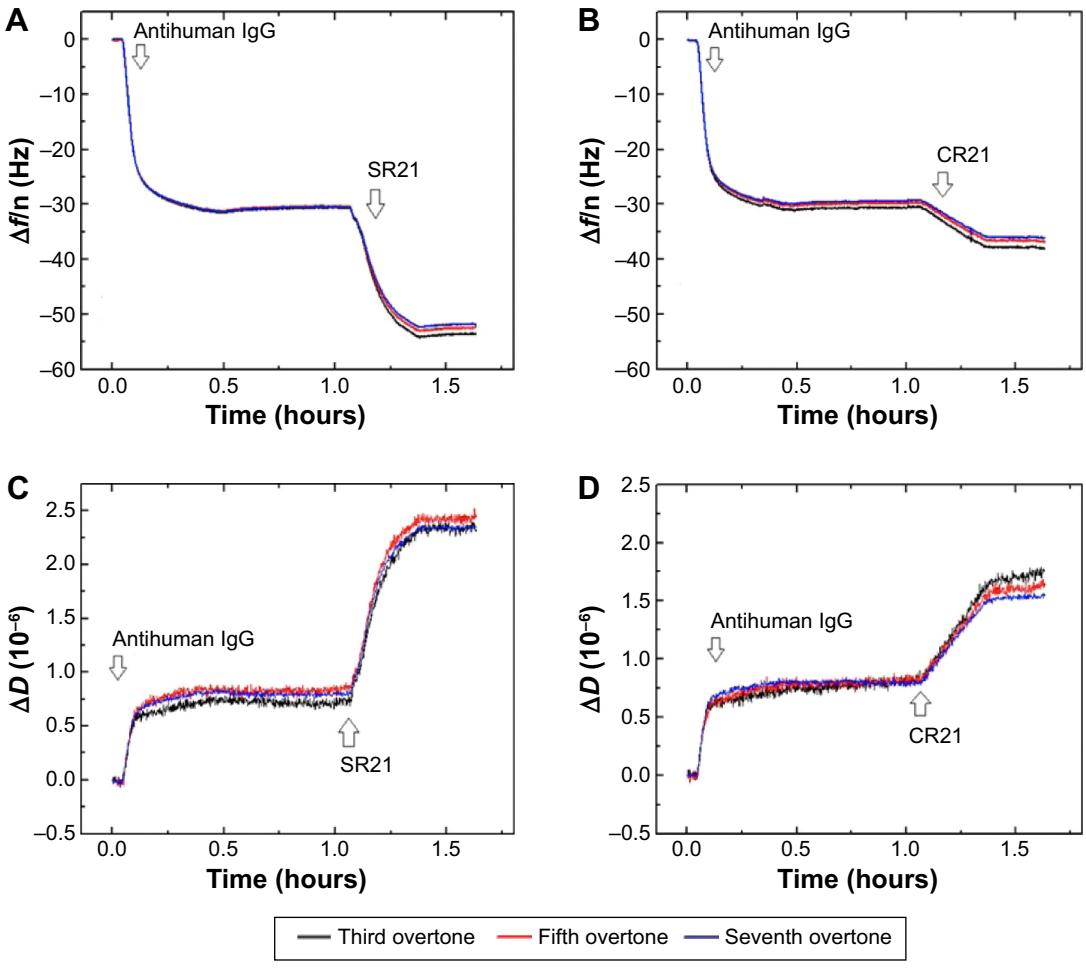

Figure 5 Characterization of antihuman IgG adsorption and subsequent binding of positive complex (**A** and **C**) and negative complex (**B** and **D**) to the Au-coated QCM-D sensors. The arrows indicate the time of addition of the sample.
Abbreviation: QCM-D, quartz crystal microbalance with dissipation monitoring.

layer) showed very similar Δf and ΔD responses in all four sensors, confirming the same kind of IgG adsorption and layer formation in all four Au crystals.

Subsequent introduction of the positive phage complex results in larger shifts in Δf and ΔD. The Δf response changes in absolute value ~25 Hz, while ΔD increases an amount of ~2×10^{-6}. When the negative complex is added, Δf decreases ~5 Hz and ΔD increases ~0.75×10^{-6}. The positive phage complex shows a larger Δf response than the negative phage complex, indicating larger mass binding to the IgG layer. This is due to the specific binding between the phage bound autoantibodies and the antihuman IgG adsorbed surfaces. The display of autoantigenic target on the phage pVI via the phagemid system will allow ~10% of the phage to display the target, in contrast to the SBP display via helper plasmid system, which can display SBP in all phages.[11] Hence, the Δf decrease is much lower compared to phage immobilization in Figure 1. The binding of the negative complex was considered as nonspecific, since the surface was not blocked beforehand. Figure 6 shows ΔD – Δf plots with different k_{D-f} slopes upon antihuman IgG and phage addition stages. The low k_{D-f} values obtained during the formation of antihuman IgG layer for both positive and negative complexes are very similar (k_{D-f} ~–0.03) and indicate that the antihuman IgG layer is rigid. In contrast, phage binding represented a higher value for both the positive and negative complexes. An effective thickness obtained using the Voigt based model reflects a significant increase in thickness upon phage binding (Figure 6C and D). Unlike binding of SBP displaying phage and STV interaction, where the phage conformation at the surface was likely vertical with very large ΔD and k_{D-f} values, the binding of phage to antihuman IgG via the autoantibody biomarker results in lower ΔD, k_{D-f}, and thickness values. These difference can be related to their conformation on the surface, the phage adopts a vertical configuration when bound to the STV layer that can be largely

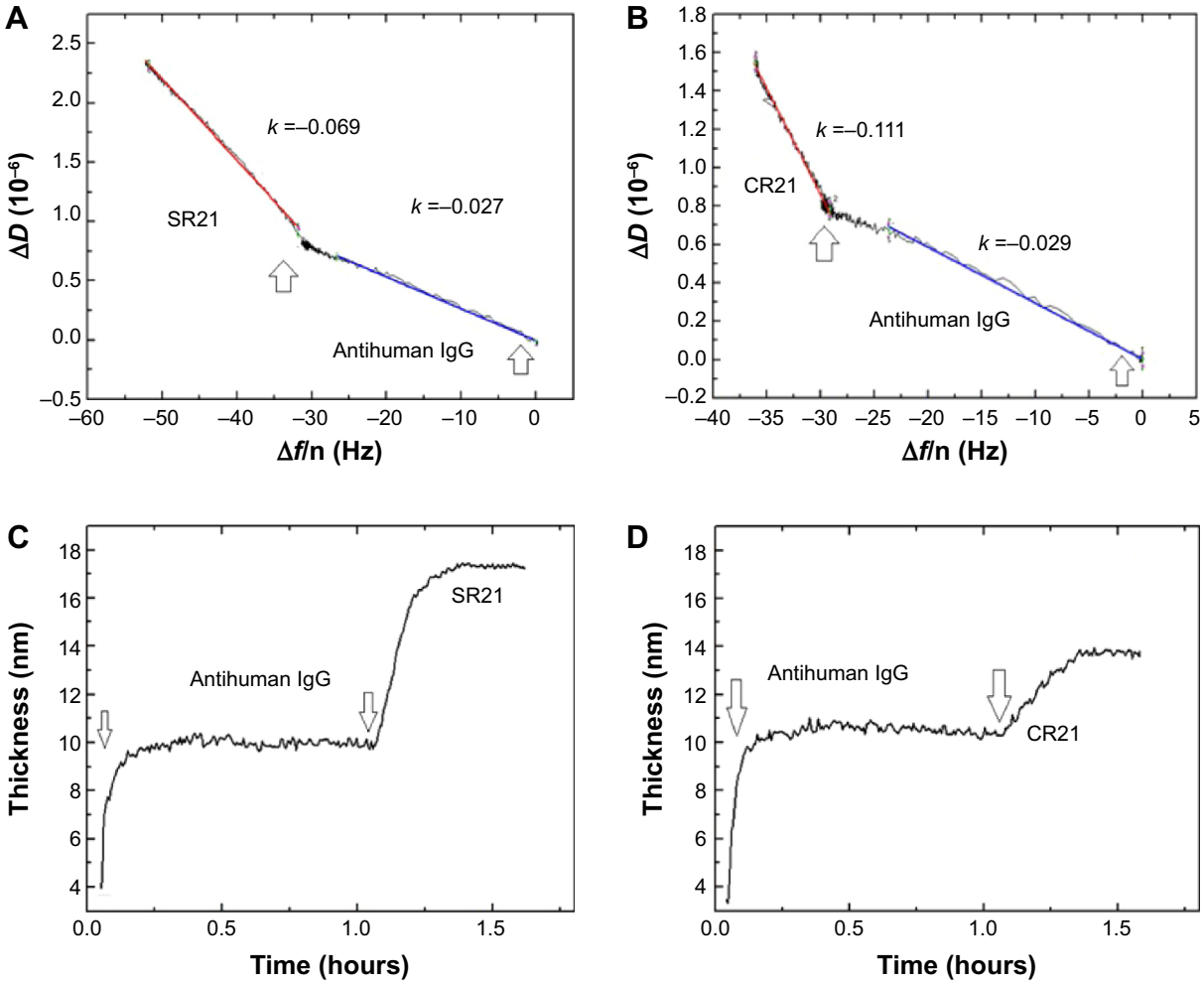

Figure 6 Binding of positive and negative complexes onto the antihuman IgG surface.
Notes: ΔD – Δf plots for overtone seven on antihuman IgG adsorption (blue solid line is a linear fit with slope k_{D-f}) and binding of positive complex (**A**) and negative complex (**B**) (red solid line is a linear fit with slope k_{D-f}). (**C** and **D**) Estimated thickness of the positive complex and the negative complex layers, respectively. The arrows indicate the time of addition of the sample.

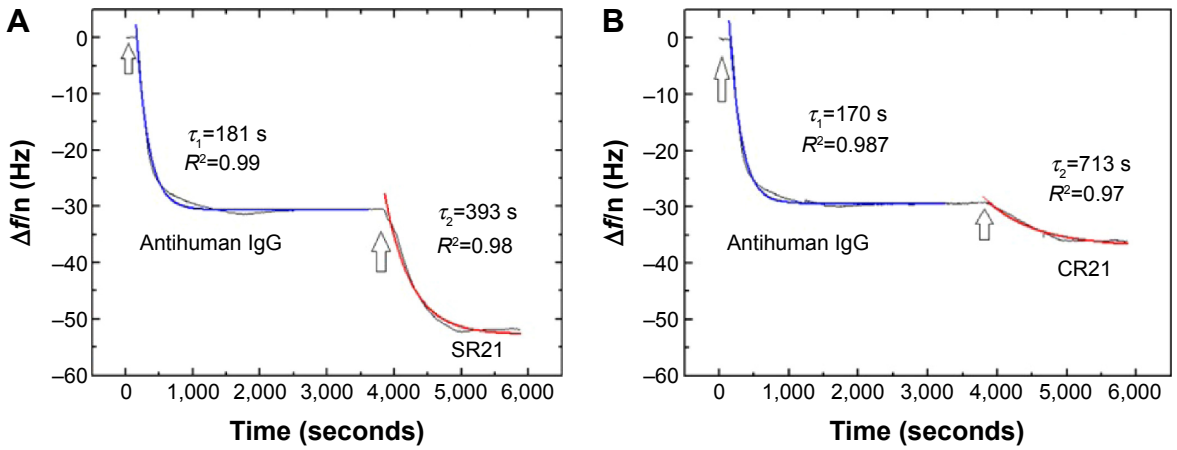

Figure 7 Kinetic study on adsorption of IgG to Au-coated QCM-D sensors and subsequent binding of positive complex (**A**) and negative complex (**B**) for overtone seven.
Notes: The solid lines represent the fits to Equation 1: $\Delta f = \Delta f_0 + Ae^{-t/\tau}$. The arrows indicate the time of addition of the sample.
Abbreviations: QCM-D, quartz crystal microbalance with dissipation monitoring; *A*, amplitude; τ, time constant.

deformed during the shear oscillation, whereas when bound to the antihuman IgG layer, less phage complex is bound being more rigid and does not accommodate vertically due to the presence of a heavy magnetic bead on the opposite end. The time constants obtained by fitting the Δf data to Equation 1 in Figure 7 indicates that IgG adsorption onto Au surface is a fast process (τ ~180 seconds). In addition, the subsequent binding of the positive complex to antihuman IgG was happened faster (τ~393 seconds) as compared to the nonspecific binding of the negative complex (τ ~713 seconds).

Conclusion

In this work, we used QCM-D to follow in real time the binding of a novel dual-display phage with different end functionalities, SBP at one end and a rheumatoid arthritis biomarker at the other end. Four phages displaying different end functionalities were used for the sake of better comparison. When binding via the SBP end to a STV-modified gold surface, the phage displaying adopt a flexible, vertical conformation, characterized by large frequency and dissipation shifts and a large effective thickness. Phage binding takes place gradually and slower compared to an STV layer formation on gold. Negative control phage that is nondisplayer of SBP shows no binding response on STV-modified gold surfaces. Complementary SPR measurements confirm the high affinity between SBP and STV by displaying large response units.

The detection of autoantibodies in the antihuman IgG immobilized surfaces was carried out using phage complex made up of a dual-display phage, STV-coated magnetic beads, and serum samples. Patient's serum sample containing autoantibodies was bound to the dual-display phage's autoantigenic target UH-RA.21 and at the same time SBP of the dual-display phage bound to the magnetic beads, thus making a positive complex. In turn, the healthy control serum, which had no serum autoantibody could not make a complex. Autoantibodies in the positive complex specifically bound to the antihuman IgG immobilized surfaces and resulted into larger frequency and dissipation shifts than the negative complex that contains no autoantibody (Figure S3).

While comparing the phage functionalization over the STV surface of QCM-D crystals and the phage complex binding to the antihuman IgG surface, lower dissipation and frequency changes were observed for the later. The lower dissipation can be ascribed to the fact that heavy magnetic beads in the complex bring down the vertically oriented phage, making it less dissipative. The lower mass adsorbed is due to the fact that phagemid-based display systems in which autoantigenic target is displayed, show a very low display level (~10% of the dual-display phage will have UH-RA.21), leading to a low number of complex binding over the sensor surface.

Further improvements would require blocking of the surface to avoid undesired nonspecific binding. These results prove that this dual-display phage can be used in isolating any protein of interest from complex mixtures and could be a better alternative to the phage ELISA protocols in qualitatively detecting the presence of autoantibodies in patient's serum sample. In the future, this work can be taken as a reference to use this novel type of dual display as a label-free diagnostic tool into rapid, highly sensitive sensing platforms in analyzing patient's serum samples.

Acknowledgments

The authors thank Mrs Igna Rutten and Ms Lotte Vanbrabant for their technical assistance. We also thank Hasselt University

for funding this project through the grant 08GO2BOF. The authors also would like to thank Professor Ana Losada for her time in proofreading the manuscript.

Disclosure

The authors report no conflicts of interest in this work.

References

1. Arap MA. Phage display technology. Applications and innovations. *Genet Mol Biol*. 2005;28(1):1–9.
2. Mao C, Liu A, Cao B. Virus based chemical and biological sensing. *Angew Chem Int Ed Engl*. 2009;48(37):6790–6810.
3. Singh A, Somayyeh P, Evoy S. Recent advances in bacteriophage based biosensors for food-borne pathogen detection. *Sensors*. 2013;13(2):1763–1786.
4. Kierny MR, Cunningham TD, Kay BK. Detection of biomarkers using recombinant antibodies coupled to nanostructured platforms. *Nano Rev*. 2012;3:17240.
5. Petrenko VA. Landscape phage as a molecular recognition interface for detection devices. *Microelectronics J*. 2008;39(2):202–207.
6. Tolba M, Minikh O, Brovko LY, Evoy S, Griffiths MW. Oriented immobilization of bacteriophages for biosensor applications. *Appl Environ Microbiol*. 2010;76(2):528–535.
7. Reynolds F, Panneer N, Tutino CM, et al. A functional proteomic method for biomarker discovery. *PLoS One*. 2011;6(7):e224771.
8. Soendegaard M, Newton-Northup JR, Palmier MO, Deutscher SL. Peptide phage display for discovery of novel biomarkers for imaging and therapy of cell subpopulations in ovarian cancer. *J Mol Biomark Diagn*. 2011;S2:004.
9. Nakanishi K, Sakiyama T, Kumada Y, Imamura K, Imanaka H. Recent advances in controlled immobilization of proteins onto the surface of the solid substrate and its possible applications to proteomics. *Curr Proteomics*. 2008;5(3):161–175.
10. Somers K, Geusens P, Elewaut D, et al. Novel autoantibody markers for early and seronegative rheumatoid arthritis. *J Autoimmun*. 2011;36:33e46.
11. Woo MK, Heo CK, Hwang HM, Ko JH, Yoo HS, Cho EW. Optimization of phage immobilized ELISA for autoantibody profiling in human sera. *Biotechnol Lett*. 2011;33:655–661.
12. Rajaram K, Vermeeren V, Somers K, Somers V, Michiels L. Construction of a helper plasmid-mediated dual-display phage for autoantibody screening in serum. *Appl Microbiol Biotechnol*. 2014;98(14):6365–6373.
13. Chen H, Su X, Neoh KG, Choe WS. QCM-D analysis of binding mechanism of phage particles displaying a constrained heptapeptide with specific affinity to SiO2 and TiO2. *Anal Chem*. 2006;78(14):4872–4879.
14. Becker B, Cooper MA. A survey of the 2006–2009 quartz crystal microbalance biosensor literature. *J Mol Recognit*. 2011;24(5):754–787.
15. Elmlund L, Söderberg P, Suriyanarayanan S, Nicholls IA. A phage display screening derived peptide with affinity for the adeninyl moiety. *Biosensors*. 2014;4(2):137–149.
16. Sauerbrey G. The use of oscillators for weighting thin layers and for microweighting. *Z Phys C Part Fields*. 1959;155:206–212.
17. Höök F, Rodahl M, Kasemo B, Brzezinski P. Structural changes in hemoglobin adsorption to solid surfaces: effects of pH, ionic strength, and ligand binding. *Proc Natl Acad Sci U S A*. 1998;95(21):12271–12276.
18. Losada-Pérez P, Khorshid M, Hermans C, et al. Melittin disruption of raft and non-raft-forming biomimetic membranes: a study by quartz crystal microbalance with dissipation. *Colloids Surf B Biointerfaces*. 2014;123:938–944.
19. Sandberg T, Carlsson J, Ott MK. Interactions between human neutrophils and mucin-coated surfaces. *J Mater Sci Mater Med*. 2009;20(2):621–631.
20. Voinova MV, Jonson M, Kasemo B. Dynamics of viscous amphiphilic films supported by elastic solid substrates. *J Phys Condens Matter*. 1997;9(37):7799–7808.
21. Losada-Pérez P, Jiménez-Monroy K, van Grinsven B, et al. Phase transitions in lipid vesicles detected by a complementary set of methods: heat-transfer measurements, adiabatic scanning calorimetry and quartz crystal microbalance. *Phys Status Solidi A*. 2014;211(6):1377–1388.
22. Rich RL, Myszka DG. Higher-throughput, label-free, real-time molecular interaction analysis. *Anal Biochem*. 2007;36(1):1–6.
23. Swann MJ, Peel LL, Carrington S, Freeman NJ. Dual-polarization interferometry: an analytical technique to measure changes in protein structure in real time, to determine the stoichiometry of binding events, and to diVerentiate between speciWc and nonspeciWc interactions. *Anal Biochem*. 2004;329:190–198.
24. Lin Z, Wang X, Li ZJ, et al. Development of a sensitive, rapid, biotin-streptavidin based chemiluminescent enzyme immunoassay for human thyroid stimulating hormone. *Talanta*. 2008;75:965–972.

Supplementary materials

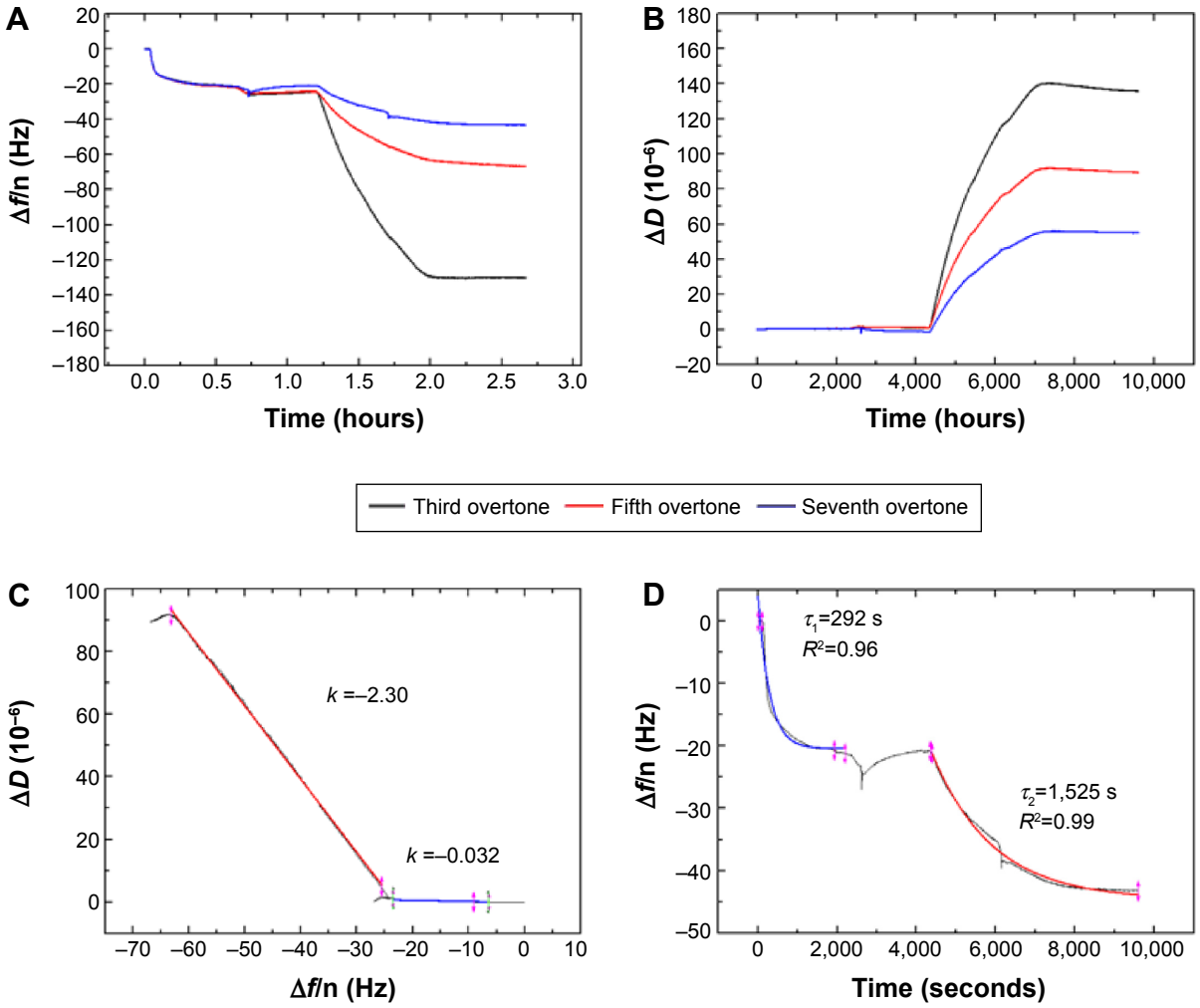

Figure S1 STV adsorption on Au-coated QCM-D sensors and subsequent binding of SBP displaying phage SB.
Notes: (**A** and **B**) Show the Δf and ΔD responses, respectively, and (**C** and **D**) representing the kinetics study on the STV and SB phage binding.
Abbreviations: STV, streptavidin; QCM-D, quartz crystal microbalance with dissipation monitoring; SBP, streptavidin-binding protein.

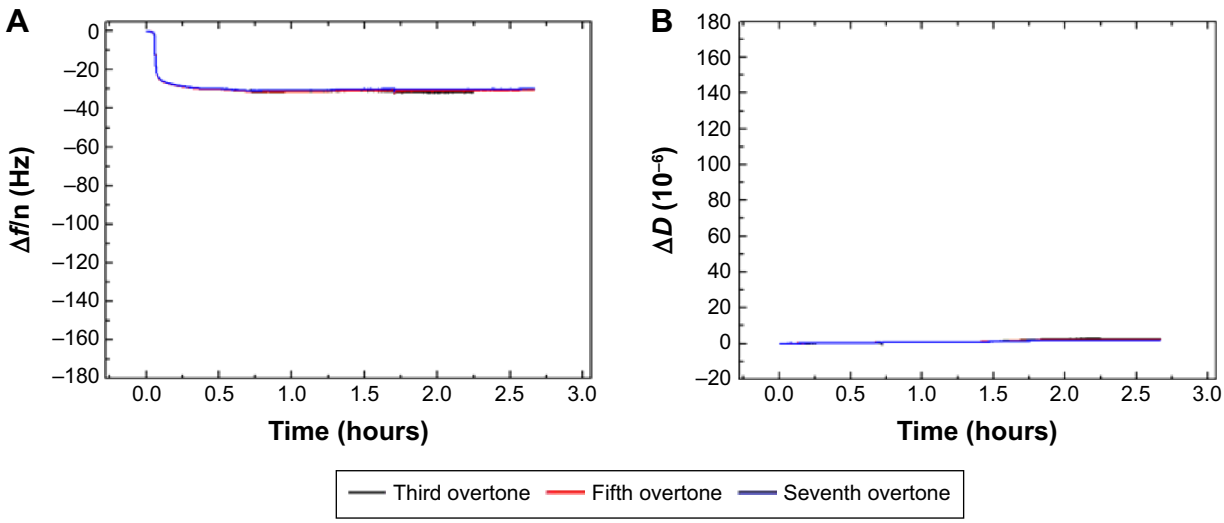

Figure S2 STV adsorption on Au-coated QCM-D sensors and subsequent binding of non-SBP displaying phage CB.
Notes: (**A** and **B**) Show the Δf and ΔD responses, respectively.
Abbreviations: STV, streptavidin; QCM-D, quartz crystal microbalance with dissipation monitoring; SBP, streptavidin-binding protein.

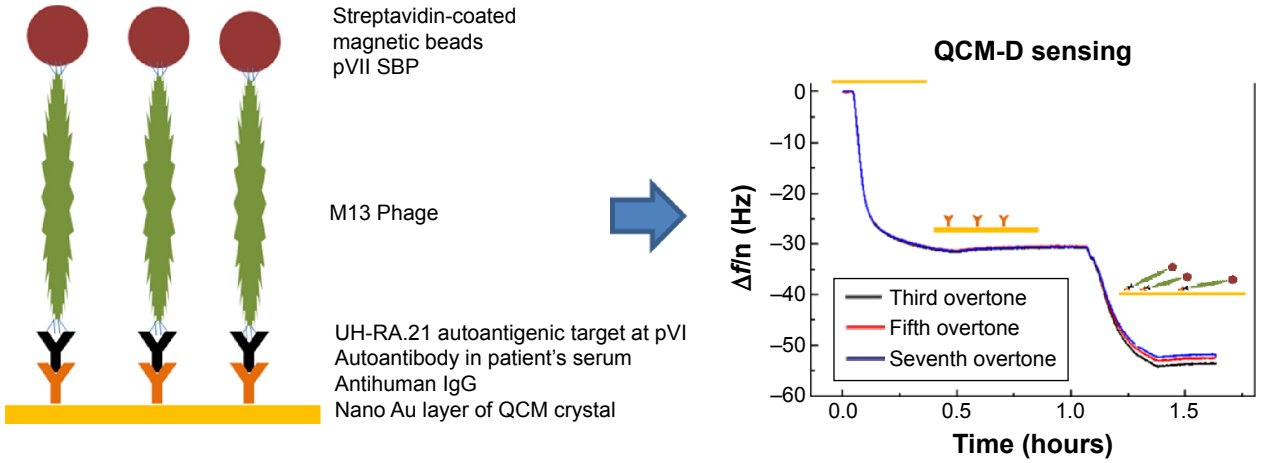

Figure S3 Schematic diagram of the dual-display phage sensor and the change in the frequency Δf with time upon binding of antihuman IgG and the phage complex on QCM-D.
Abbreviations: QCM-D, quartz crystal microbalance with dissipation monitoring; SBP, streptavidin-binding protein.